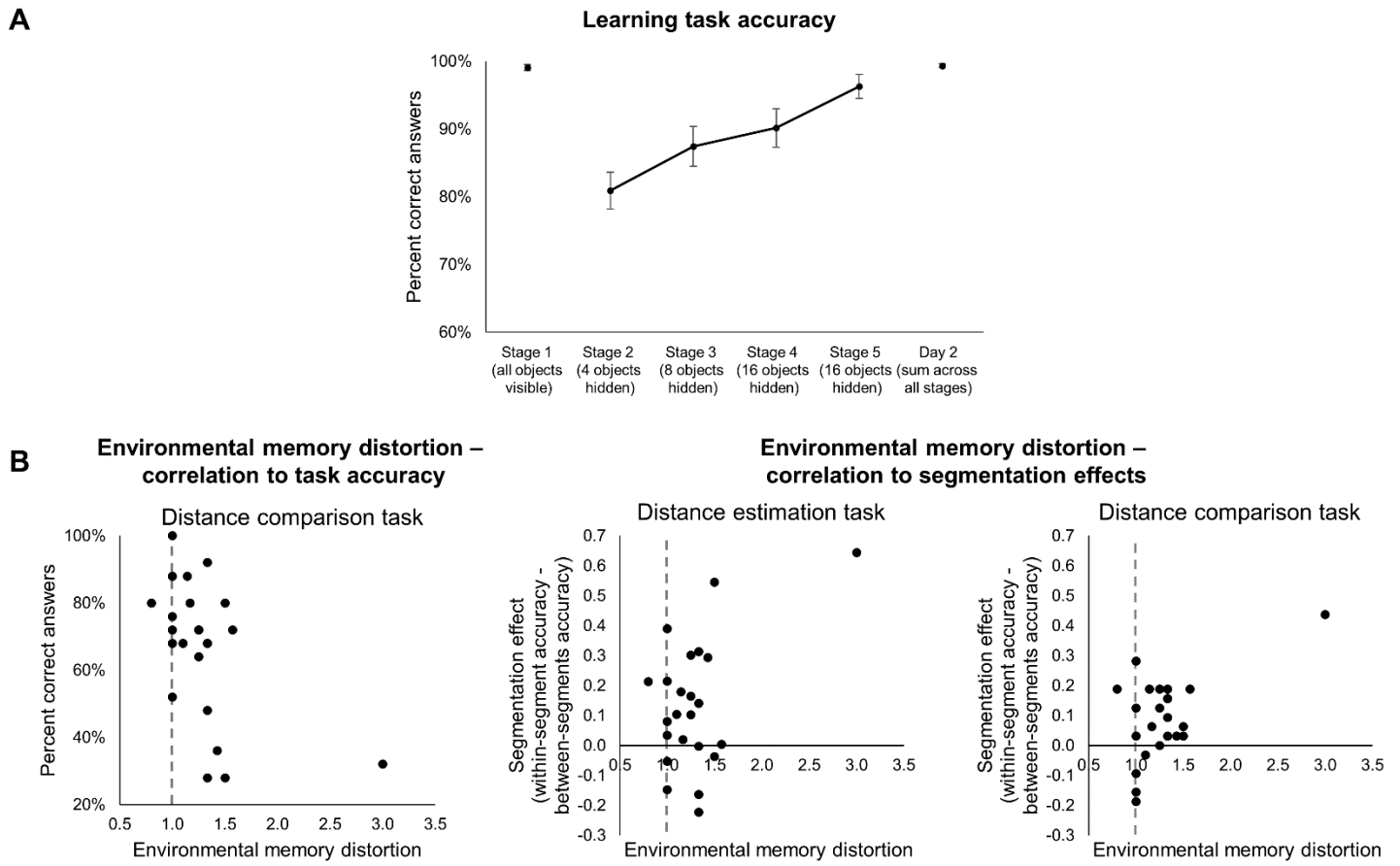

Figure S1: Additional behavioral results, related to Figure 2. A) Learning of the virtual environment. The fraction of objects found without mistakes is plotted for each stage of the environmental learning task. Performance was near ceiling with all object visible in stage 1. Performance was lower in stage 2 when four objects including the target were covered by planks so that they were not visible, but improved gradually over subsequent stages, despite the increasing number of objects obscured. By stage 5, participants could find most objects without error even with all objects obscured. On day 2, participants performed 10 minutes of the learning task, starting again from the beginning. They performed close to ceiling, indicating full learning of object locations. Circles indicate mean accuracy across participants; error bars ±1 standard error of the mean.

B) Environmental memory distortion effects. We asked participants to estimate the size of the environment along each direction. Sixteen participants believed that the environment was more elongated along the river direction, one participant thought that the environment was elongated in the direction perpendicular to the river, and the remaining seven participants accurately identified the environment as square. It is interesting that the majority of participants thought that the environment was elongated along the river rather than across it, given that their distance estimates would suggest the opposite pattern. The amount of distortion was then quantified using by dividing the north-south (along river) estimated length by the east-west estimated length, resulting in a directional measure in which 1 indicates no memory distortion, <1 indicate memory elongation along the east-west axis, and >1 indicates elongation along the north-south axis. This distortion index was negatively correlated with accuracy in the distance comparison task ($r=-0.51$, $p=0.013$, left), and positively correlated with segmentation effects in the distance estimation task ($r=0.47$, $p=0.025$, middle) and distance comparison task ($r=0.56$, $p=0.006$, right). Thus, participants who had a more distorted memory for the shape of the environment made distance judgments that were less accurate and more segmented. However, these effects were strongly influenced by an outlier participant who remembered the environment as three times longer along the North/South axis. When this participant was excluded, correlations dropped to $r=-0.42$ for distance estimation accuracy ($p=0.052$), and $r=0.03,0.20$ for distance estimation and distance comparison segmentation effects (both $Ps>0.37$).

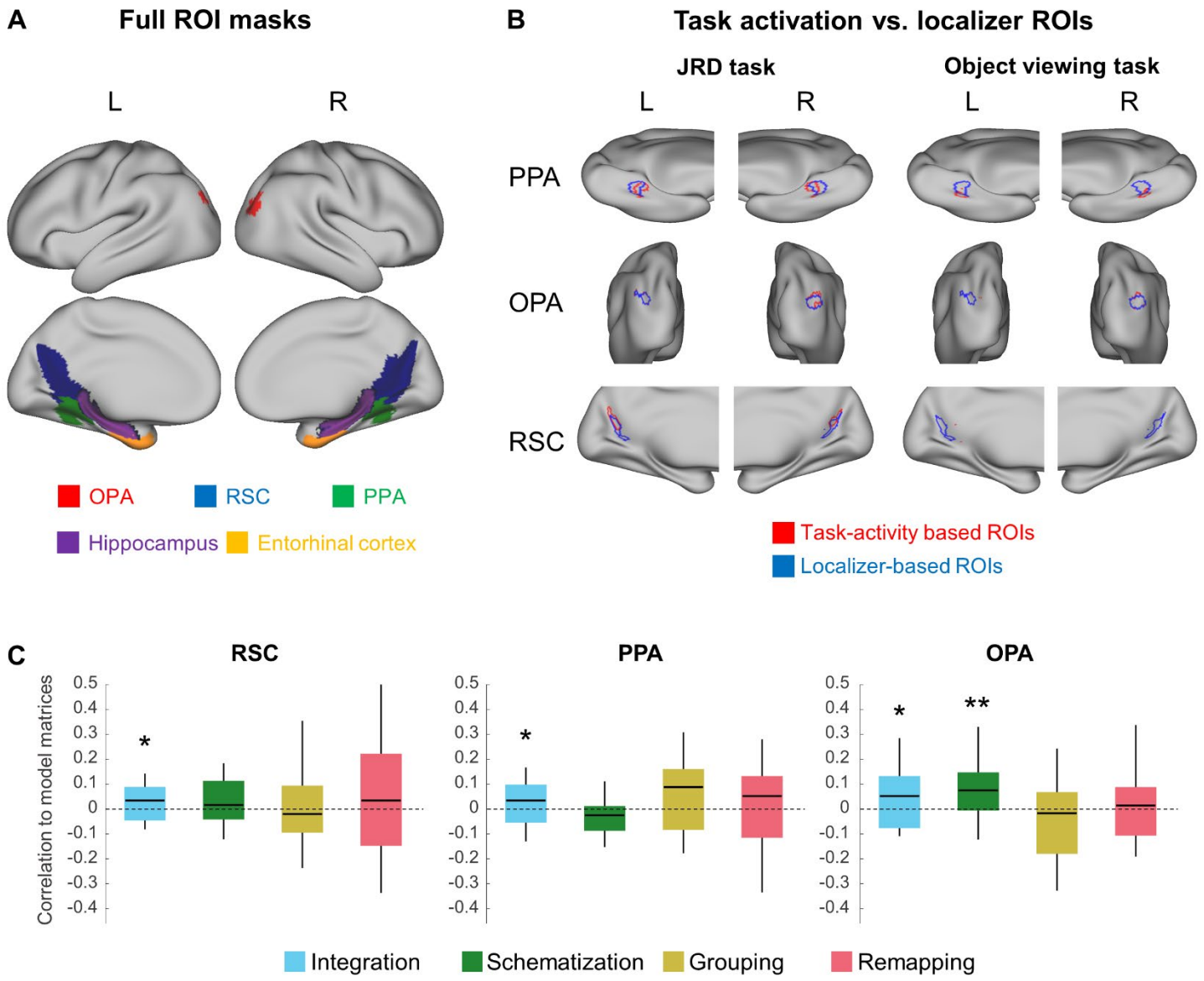

Figure S2: Region of interest (ROI) masks and relation between task-based and localizer-based ROIs, related to STAR Methods section "Definition of regions of interest". A) We used parcels from [S1] to define the occipital place area (OPA, red), retrosplenial complex (RSC, blue), and parahippocampal place area (PPA, green). These parcels were used in combination with functional data to identify participant-specific ROIs. The hippocampus (purple) and entorhinal cortex (orange) were defined anatomically based on freesurfer parcellations. B) To define task-based ROIs, we selected voxels within the PPA, OPA, and RSC parcels that showed the greatest activation relative to baseline during the JRD and object viewing tasks. These task-based voxels (red) were different but partially overlapping with the voxels that showed greatest scene-selective activity in an independent perceptual localizer (blue), corroborating previous findings[S2–6]. In PPA the localizer-based ROI tended to be more posterior than the task-based ROI for the JRD task and more medial than the task-based ROI for the object viewing task. In OPA, the localizer- and task-based ROIs were largely overlapping. In RSC, the localizer-based ROI tended to be more ventral and posterior than the JRD task-based ROI. Colored voxels indicate voxels that were selected for at least 6 out of the 24 participants; in the RSC in the object viewing tasks, no voxels passed this threshold. C) Integration and segmentation effects in localizer-defined ROIs. In the JRD task, the integration and schematization models were significant in OPA (Z=1.99,2.92, p=0.046,0.006, effect size r=0.42,0.61, respectively), and the integration model was significant in RSC (Z=1.84, p=0.046, effect size r=0.38), corroborating the results of the main analysis in the activation-based ROIs. There was also a significant integration effect in PPA (Z=1.66, p=0.049, effect size r=0.35), which had been only marginally significant in the main analysis. No effects were significant in the localizer-based ROIs in the object viewing task (all ps>0.05). Box plot elements are the same as in Figure 2. Asterisks represent significant effects (one-tailed one-sample Wilcoxon signed-rank test for each model in each ROI, FDR-corrected for multiple comparisons across ROIs). RSC – retrosplenial complex, PPA – parahippocampal place area, OPA – occipital place area.

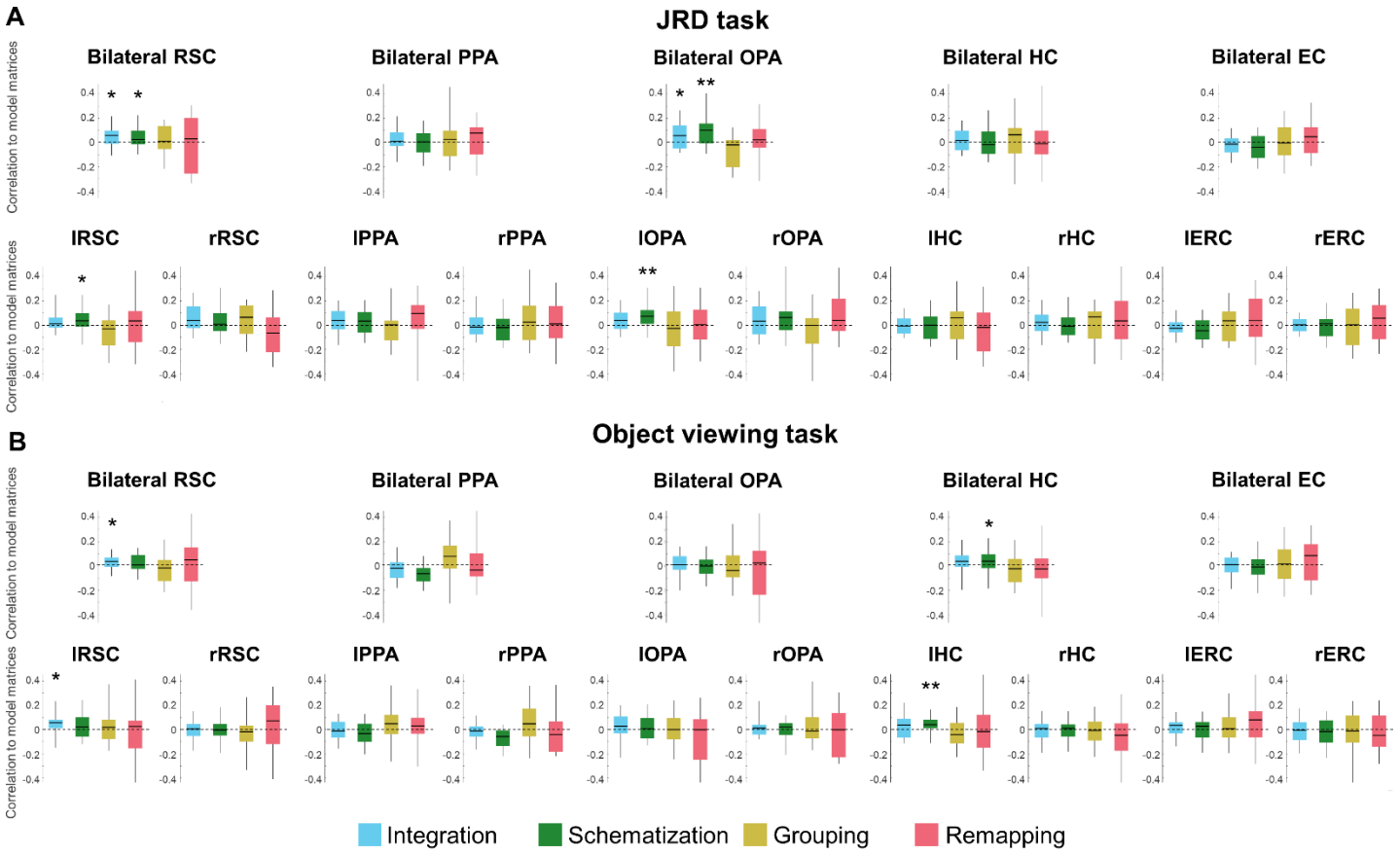

Figure S3: Model fits in all bilateral and unilateral ROIs, related to Figure 4. In addition to the main analyses on bilateral ROIs described in the main text, we conducted exploratory analyses to test the observed effects in each brain hemisphere separately. A) In the JRD task, correlation of neural RDMs to the schematization model was significant in left RSC and left OPA, and close to significance in right OPA (Z=2.42,3.36,2.05; p=0.039,0.004,0.067; effect size r=0.50,0.70,0.43, respectively). The integration model was marginally significant in right RSC (p=0.086). B) In the object viewing task, correlation of the neural RDM to the integration model was significant in left RSC (Z=2.74, p=0.029, effect size r=0.57), and correlation to the schematization model was significant in left hippocampus (Z=3.23, p=0.004, effect size r=0.69). The grouping and remapping models did not predict neural similarities in any unilateral ROI (all ps>0.1). r – right hemisphere, l – left hemisphere, RSC – retrosplenial complex, PPA – parahippocampal place area, OPA – occipital place area, HC – hippocampus, ERC – entorhinal cortex. Asterisks represent significant effects (one-tailed one-sample Wilcoxon signed-rank test for each model in each ROI, p-values for each task are FDR-corrected for multiple comparisons across all five bilateral ROIs or ten unilateral ROIs). Box plot elements are the same as in Figure 2.

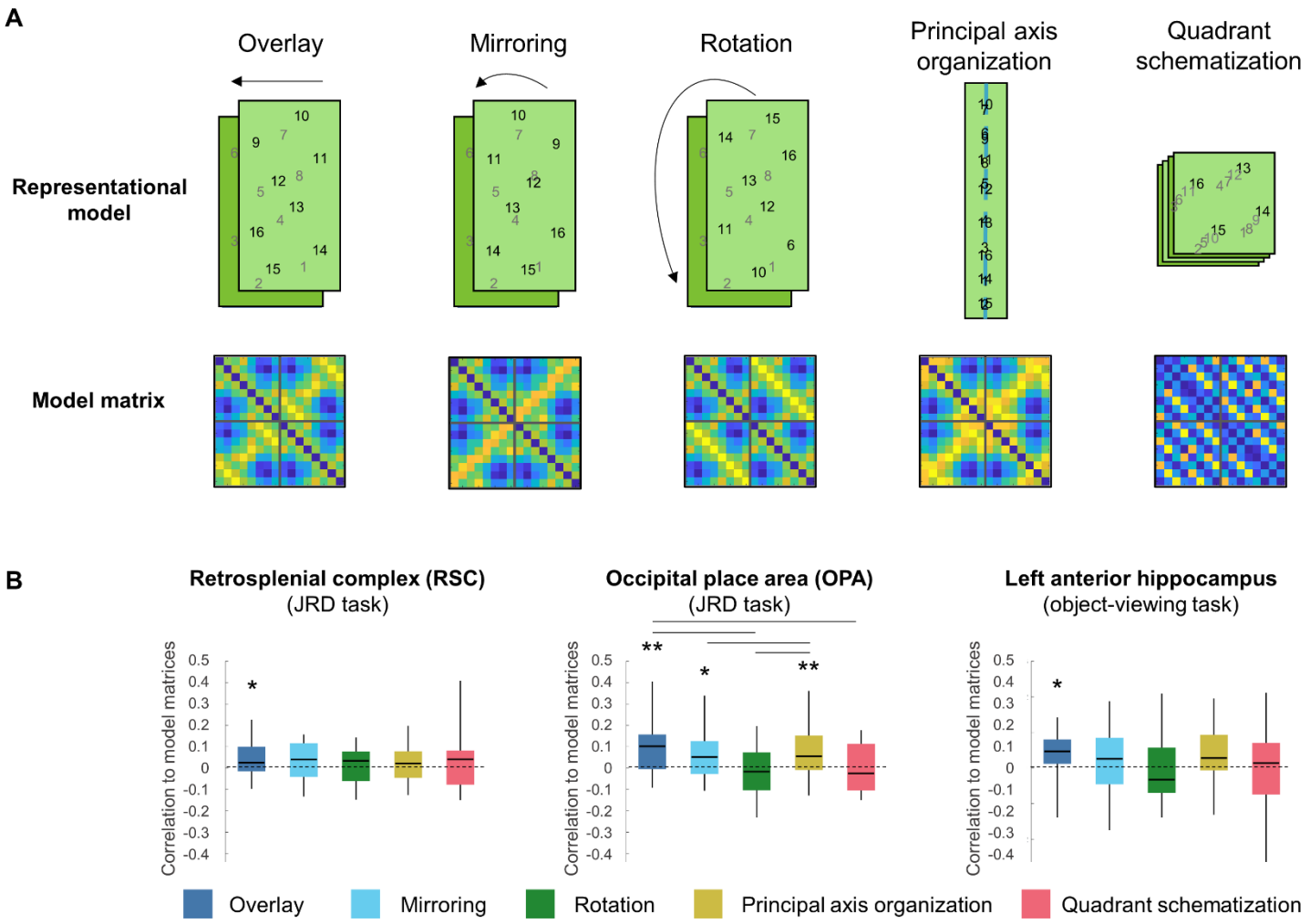

Figure S4: Comparison of different schematization models, related to Figure 4. A) Schematization implies that neural representations are overlapping between the two segments. However, different types of schematization are possible. To test alternative forms of schematization, we constructed object distance matrices under three different models: overlay (the schematization model described in the main text), mirroring (flipping of the segments along the river axis so that they are overlaid as a mirror image of each other), and rotation (overlay of the segments with 180 degrees rotation). We also tested a fourth schematization model in which stimuli are represented solely in terms of their location along the principal environmental axis defined by the direction of the river and the distal landmarks. Finally, we tested a model of quadrant schematization, under which the four quadrants are represented as overlaid on each other. Note that the overlay model is highly similar to the mirroring and principal axis models in terms of inter-object distances (r=0.93, 0.97, respectively), and therefore it is difficult to disambiguate their effects from each other; however, these three models were not highly correlated to the rotation or quadrant schematization models (all rs<0.19). B) Correlation of the different models to neural similarities in RSC, OPA, and left anterior hippocampus. Neural similarities during the JRD task were significantly correlated with the overlay model in RSC (Z=2.27, p=0.029, effect size r=0.71) and significantly correlated with the overlay, mirroring, and principal axis models in OPA (Z=2.27, 2.47, 3.00, p=0.002, 0.036, 0.007, effect size r=0.71, 0.51, 0.62 respectively). Neural similarities during the object viewing task were significantly correlated with the overlay model in the left anterior hippocampus (Z=2.99, p=0.011, effect size r=0.61), and the correlation to the principal axis model was close to significance in this region (Z=2.47, p=0.053, effect size r=0.50). The rotation and quadrant schematization models did not significantly fit the data in any ROI (all ps>0.43). The five models had significant differences in their fit to the data in the OPA, with the overlay model providing the best overall fit which was significantly better than the rotation or quadrant schematization models (p=0.03,0.03, paired-samples Wilcoxon signed rank tests, FDR-corrected for multiple comparisons), but there were no significant differences in the RSC or left anterior hippocampus (all ps>0.2). Asterisks represent significant effects (one-tailed one-sample Wilcoxon signed-rank test for each model in each ROI, FDR-corrected for multiple comparisons across ROIs). Lines indicate significant differences between models (pairwise Wilcoxon signed rank tests, FDR-corrected for multiple comparisons across models). Box plot elements are the same as in Figure 2.

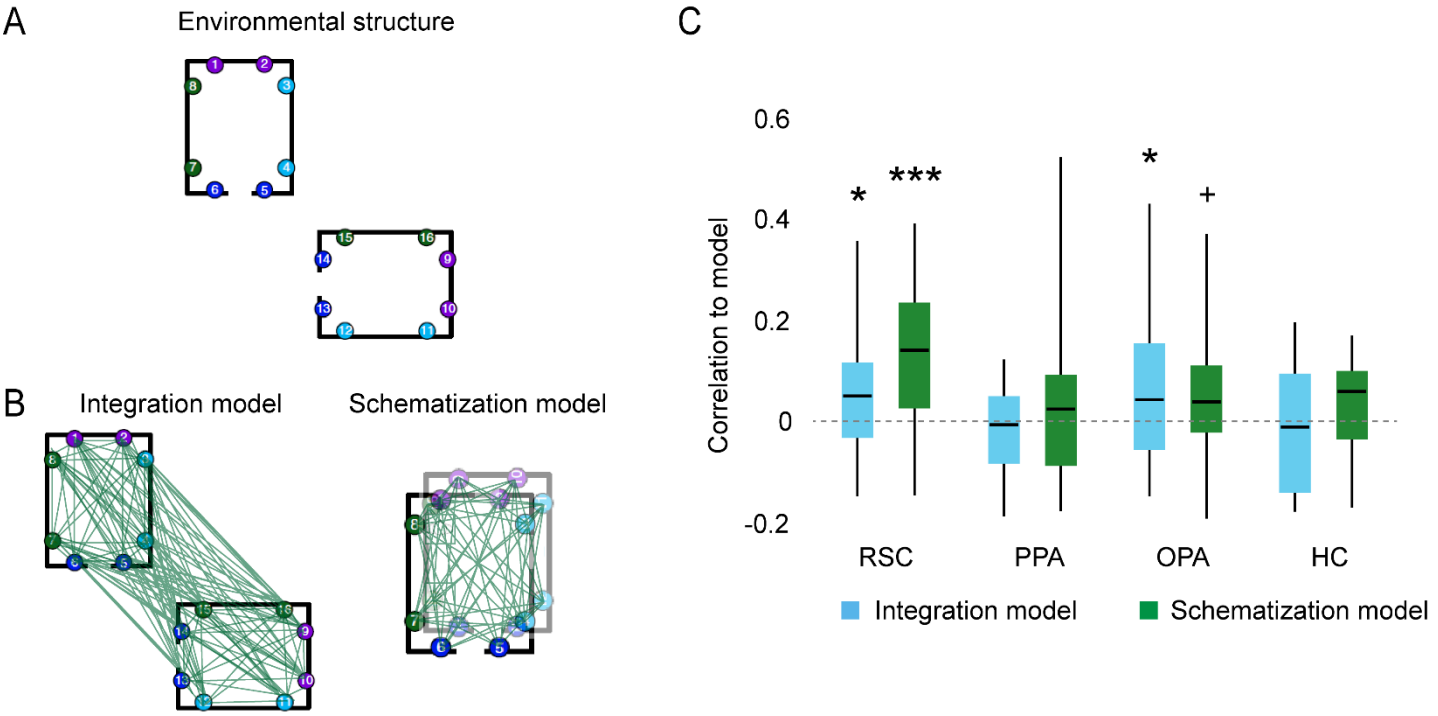

Figure S5: Schematization across spatial segments – replication in independent data, related to STAR Methods section "Re-analysis of data from Marchette et al. 2014". A) Participants in a previous study[S7] were familiarized with a virtual environment consisting of four buildings arrayed in a cross-like pattern within a courtyard. Each building had a single entrance, and the interiors of all the buildings had the same rectangular shape. Within each building were eight unique objects, located in fixed positions along the walls, indicated here by numbered circles. After environmental familiarization, participants performed a JRD task in which they imagined themselves standing in front of the objects from two of the four museums. Thus, the design of the previous study was similar to the current one, but with three notable differences: (i) the subspaces in the previous study were delineated by walls rather than by a river that afforded co-visibility; (ii) the subspaces were aligned perpendicularly rather than in parallel; (iii) each object was imagined from a single direction rather than a variety of directions.

B) We previously[S7] reported results from classification analyses on multivoxel patterns, which revealed evidence for spatial codes in RSC that generalized across the building interiors—consistent with schematization. Here we more formally test the schematization and integration models by performing representational similarity analyses. Lines indicate distances between the objects that were used to construct representational similarity matrices.

C) Neural pattern similarities in RSC were significantly correlated to both the integration model ($Z=2.21$, $p=0.027$, effect size $r=0.45$, FDR-corrected for multiple comparisons over ROIs) and the schematization model ($Z=3.5$, $p=0.0009$, effect size $r=0.71$), but the schematization model provided a significantly better fit ($t(23)=2.03$, $p=0.04$, effect size $r=0.41$). Neural pattern similarities in OPA were significantly correlated to the integration model ($Z=2.36$, $p=0.027$, effect size $r=0.48$) and marginally correlated to the schematization model ($Z=1.9$, $p=0.057$, effect size $r=0.39$), but with no significant difference between model fits ($Z=0.57$, $p=0.57$, effect size=0.12). This finding of spatial coding of OPA is notable because it was not revealed by the classification analyses used in the previous report. There were no significant effects in PPA or hippocampus. Asterisks represent significant correlation across participants ($p<0.05$, FDR-corrected); the plus sign indicates that correlation in OPA to the schematization model was close to significance ($p=0.057$). RSC – retrosplenial complex, PPA – parahippocampal place area, OPA – occipital place area, HC – hippocampus. Box plot elements are the same as in Figure 2.

These results show additional evidence for both schematization and integration in scene regions for an environment that is divided into subspaces. It is notable that the strongest schematization effects in the previous study were observed in RSC, whereas in the current study the strongest effects during the JRD task were observed in OPA. These differences may relate to the fact that the subspaces were defined by opaque boundaries in the previous study and the objects were all located along these boundaries. In contrast, in the current study, the subspaces were defined by a river that did not block vision, and objects were located throughout the environment. Although both sets of results confirm the importance of schematization, these differences between the studies suggest intriguing avenues for future investigation.

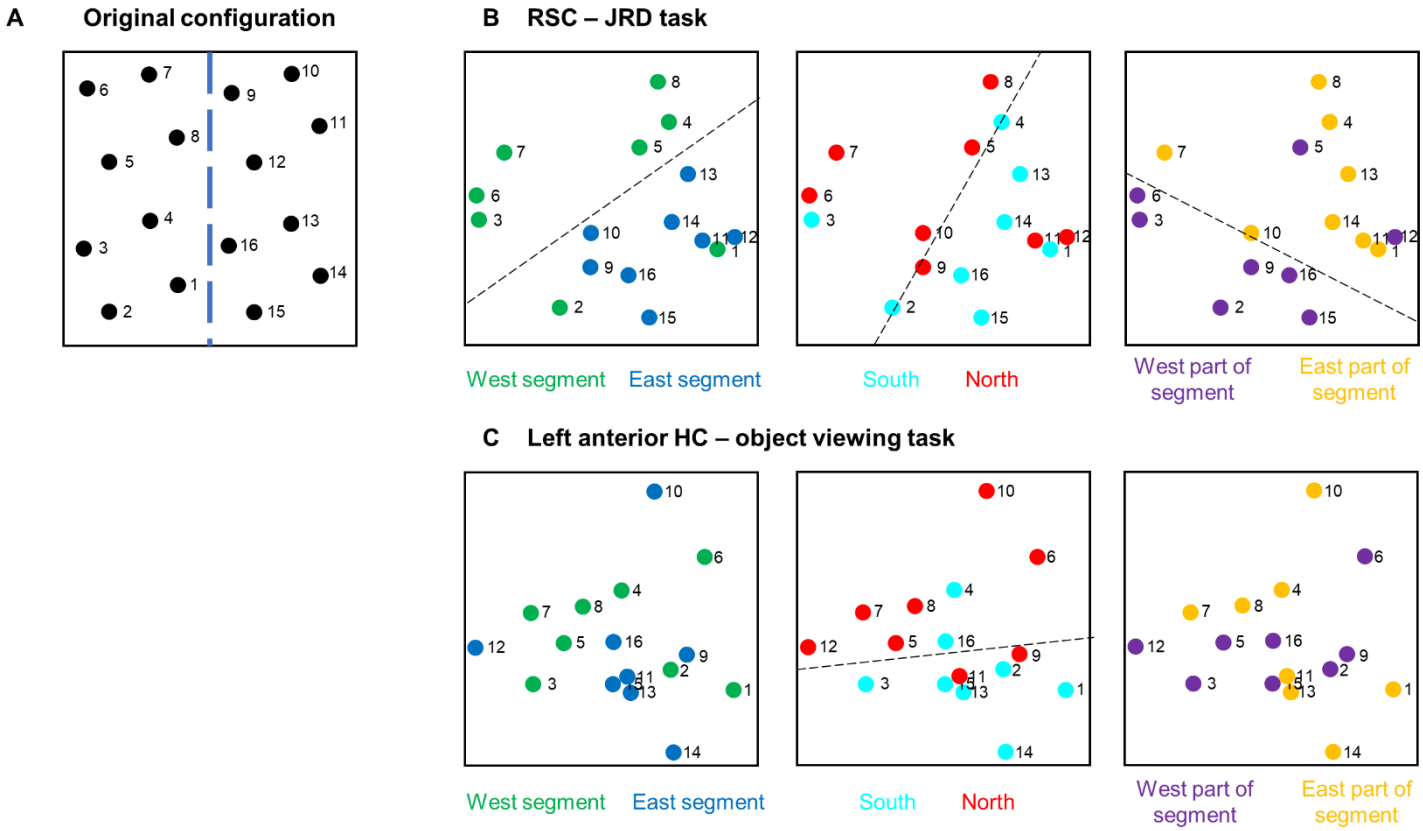

Figure S6: Multidimensional scaling demonstrates spatial organization of neural patterns in RSC and hippocampus, related to Figure 6. A) The true configuration of objects in the environment. B) Multidimensional scaling of RSC neural patterns in the JRD task data. Patterns show separation along both the north-south and east-west axes of the environment, with some evidence for overlay of patterns from each side of each segment on each other. C) Multidimensional scaling of left hippocampus neural patterns in the object viewing task data. Some evidence for organization according to location on the North/South (river) axis can be observed. See Fig. 6 legend for detailed explanation. RSC – retrosplenial complex, HC – hippocampus.

Supplemental references

S1. Julian, J.B., Fedorenko, E., Webster, J., and Kanwisher, N. (2012). An algorithmic method for functionally defining regions of interest in the ventral visual pathway. Neuroimage *60*, 2357–2364.

S2. Steel, A., Billings, M.M., Silson, E.H., and Robertson, C.E. (2021). A network linking scene perception and spatial memory systems in posterior cerebral cortex. Nat. Commun. *12*, 2632.

S3. Silson, E.H., Steel, A.D., and Baker, C.I. (2016). Scene-selectivity and retinotopy in medial parietal cortex. Front. Hum. Neurosci. *10*, 412.

S4. Burles, F., Umiltá, A., McFarlane, L., Potocki, K., and Iaria, G. (2018). Ventral-dorsal functional contribution of the posterior cingulate cortex in human spatial orientation: A meta-analysis. Front. Hum. Neurosci. *12*, 190.

S5. Baldassano, C., Esteva, A., Fei-Fei, L., and Beck, D.M. (2016). Two distinct scene-processing networks connecting vision and memory. Eneuro *3*.

S6. Baldassano, C., Beck, D.M., and Fei-Fei, L. (2013). Differential connectivity within the parahippocampal place area. Neuroimage *75*, 228–237.

S7. Marchette, S.A., Vass, L.K., Ryan, J., and Epstein, R.A. (2014). Anchoring the neural compass: coding of local spatial reference frames in human medial parietal lobe. Nat. Neurosci. *17*, 1598–1606.